





A Macro-Model for Simulating Gusset Plate Buckling in Buckling-Restrained Braced Frame Buildings

S. Sistla 🕒 | R. Chandramohan | T. J. Sullivan

Department of Civil and Natural Resources Engineering, University of Canterbury, Christchurch, New Zealand

Correspondence: S. Sistla (saiteja.sistla@pg.canterbury.ac.nz)

Received: 6 October 2024 | Revised: 7 May 2025 | Accepted: 9 May 2025

Funding: The authors received no specific funding for this work.

Keywords: buckling-restrained braced frame | collapse risk | gusset plate | non-linear dynamic analysis | seismic performance

ABSTRACT

2D models, which are conventionally employed for the seismic performance assessment of buckling-restrained braced frame (BRBF) buildings, are incapable of simulating the out-of-plane buckling of gusset plates. This study presents a novel 3D macro-modelling approach capable of capturing the out-of-plane buckling of gusset plates in BRBFs. This modelling approach is used to gain new insight into the dynamic behaviour of BRBFs by analysing a case study four-storey steel BRBF with a super-X configuration, designed using the provisions of the New Zealand seismic design standards along with guidance from practising engineers. Numerical models of the building are subjected to static pushover analysis and dynamic analyses under bidirectional hazard-consistent ground motions. The structural performance is observed to remain unaffected by gusset plate buckling up to the 2500-year return period intensity level, beyond which buckling is observed. Consideration of gusset plate buckling is found to decrease the building's deformation capacity and increase its mean annual frequency of collapse by 170%, indicating that the current NZS 3404 design procedure for gusset plates is unconservative in nature. Bidirectional loading is found to have little to no impact on the performance of the gusset plates.

1 | Introduction

Many office buildings constructed in Christchurch following the 2010–11 Canterbury earthquakes include buckling-restrained braced frames (BRBFs) [1]. Buckling-restrained braces (BRBs) have also been widely adopted across the world due to their capability to yield both in tension and compression, exhibiting fully balanced hysteresis loops and good ductility capacity. Several subassembly-level experimental studies (e.g., Vazquez-Colunga et al. [2], Tsai and Hsiao [3], Court-Patience et al. [4], Westeneng et al. [5]) have, however, highlighted the possibility of premature out-of-plane buckling of gusset plates before the BRBs can develop their full axial load-carrying capacity. Tests conducted by Vazquez-Colunga et al. [2] additionally demonstrated that gusset plate buckling was exacerbated under bidirectional loading,

resulting in a further 15% reduction in gusset plate resistance compared to unidirectional loading. Conversely, a study by Court-Patience et al. [4] reported no significant influence of bidirectional loading on gusset plate strength.

Vazquez-Colunga et al. [2], Westeneng et al. [5] and Court-Patience et al. [4] developed experimentally validated 3D continuum finite element models of BRBs with their adjoining gusset plate connections to better understand their out-of-plane buckling behaviour. Although 3D continuum models are detailed and accurate, they are computationally expensive and impractical for use in assessing the global behaviour of BRBF buildings. Hence, computationally efficient 2D macro models are often preferred instead. The 2D macro models conventionally employed to model BRBFs are limited in their ability to simulate the out-of-plane

This is an open access article under the terms of the Creative Commons Attribution-NonCommercial License, which permits use, distribution and reproduction in any medium, provided the original work is properly cited and is not used for commercial purposes.

© 2025 The Author(s). Earthquake Engineering & Structural Dynamics published by John Wiley & Sons Ltd.

buckling failure mode of gusset plates (e.g., Upadhyay et al. [6], Zsarnóczay et al. [7] and Ghowsi et al. [8]).

This study presents a novel macro-modelling approach capable of capturing the out-of-plane buckling of gusset plates in BRBFs. This approach is employed to develop the following two models of a four-storey steel BRBF building with a super-X configuration: a 3D Spatial model and a 3D Planar model. The 3D Spatial model represents a computationally efficient alternative to 3D continuum models. The 3D Planar model achieves a further improvement in computational efficiency by making a few additional simplifying assumptions. The performance of these models is compared to that of a conventional 2D model of the building. Non-linear static and dynamic analyses of these three building models are conducted to investigate the following research questions:

- 1. Can traditional modelling methods (using 2D models) be refined to effectively simulate the out-of-plane buckling failure mode of gusset plates in BRBFs?
- 2. Does bidirectional loading affect the out-of-plane buckling of gusset plates in BRBF buildings?
- 3. Does gusset plate buckling influence the estimated global seismic BRBF response?
- 4. Does gusset plate buckling influence the collapse risk of BRBF buildings?

2 | Summary of Commonly Adopted BRBF Macro-Modelling Strategies

Although a few studies (e.g., Wei et al. [9]) have developed 3D macro-models of BRBF buildings, 2D frame models are typically employed (e.g., Upadhyay et al. [6], Zsarnóczay et al. [7] and Ghowsi et al. [8]) to simulate their global seismic response, owing to their computational efficiency. The 2D BRBF modelling strategies commonly encountered in the literature are summarised in Table 1. The common elements and uniaxial material models used to model BRBs, brace-to-gusset connections, BRB frame members and the gravity system are discussed in Sections 2.1 and 2.2. Common damping modelling strategies are presented in Section 2.3.

2.1 | BRBs and Brace-to-Gusset Connections

Some studies summarised in Table 1 utilise either force- or displacement-based fibre elements [10] to model BRBs with moment-resisting and pinned brace-to-gusset connections. Force-based fibre elements employ shape functions to interpolate forces along the length of the element, whereas displacement-based fibre elements interpolate displacements. Members modelled using displacement-based fibre elements must typically be finely discretised to achieve results comparable to those obtained using a single force-based fibre element [10]. Although both element types can yield similar results, some studies (e.g., Vafaei et al. [11], Chen [12], Prinz et al. [13]) have favoured force-based fibre elements for their computational efficiency. Some studies employed truss elements to model BRBs with pinned brace-to-

gusset connections. Truss elements are more computationally efficient compared to fibre elements and have proven to be suitable for representing pin-connected BRBs, as shown by Upadhyay et al. [6] and Zsarnóczay et al. [7]. Yu et al. [14] utilised truss elements to model BRBs with moment-resisting connections; however, this modelling choice leads to an underestimation of the flexural stiffness of the BRBs and their connections. All the studies presented in Table 1 employed 2D numerical models and BRB connections were modelled as either pinned or fixed, often with rigid offsets. These approaches fall short in capturing the out-of-plane buckling of gusset plates, which may occur if gusset plate thicknesses are insufficient.

Although the Giuffré-Menegotto-Pinto steel model [15] and the bilinear model are commonly used to model the constitutive behaviour of BRBs, they cannot simulate their asymmetric constitutive behaviour. The recently proposed Zsarnóczay and Vigh steel model [7] can simulate this asymmetric constitutive behaviour, while also capping the hardening in both tension and compression. BRBs can also fracture due to low-cycle fatigue, but the Zsarnóczay and Vigh steel model cannot simulate this failure mode. It must, therefore, be used in conjunction with a fatigue material model [16] to simulate low-cycle fatigue failure.

2.2 | BRBF Beams, Columns and the Gravity System

Force- and displacement-based fibre elements with the Giuffré-Menegotto-Pinto steel model have been widely adopted to model the frame members in BRBFs. The constitutive behaviour of these frame members is symmetric and, therefore, accurately represented by this steel model. One drawback, however, is the inability of this material model to simulate the in-cycle and cyclic deterioration of strength and stiffness observed in steel structures. Some recently proposed hysteretic models (e.g., Alghossoon et al. [25] and Suzuki et al. [26]) can simulate strength and stiffness deterioration in steel members modelled using fibre elements. Alternatively, elastic beam-column elements with concentrated plastic hinges following phenomenological hysteretic rules, like the modified Ibarra-Medina-Krawinkler (IMK) model [27], have been adopted in some studies to simulate these deterioration modes. Although they are computationally efficient compared to the fibre elements, one potential drawback of concentrated plasticity models is that they are limited in their ability to capture the interaction between member axial force and bending moments. Nevertheless, Lignos et al. [28] have proposed methods to approximately account for this interaction in plastic hinge models.

Most gravity systems in steel-braced frame structures are designed with pinned column base connections and shear tab beam–column connections. The gravity columns are spliced away from the beam–column joints and, therefore, behave as continuous columns with pinned base connections. The majority of BRBF modelling strategies represent the gravity system with a leaning column that is pin-connected at every floor level and connected to the BRBF using rigid truss elements. The continuous gravity column effect is ignored in most modelling strategies (discussed in Table 1), which affects the storey drift distribution along the building height and the observed collapse mechanism [29].

10969845, 2025, 11, Downloaded from https://onlinelibrary.wiley.com/doi/10.1002/eqe.4383 by Ministry Of Health, Wiley Online Library on [15/10/2025]. See the Terms and Conditions (https://onlinelibrary.wiley.com/terms-and-conditions) on Wiley Online Library for rules of use; OA articles are governed by the applicable Ceative Commons License

				RRR to		connections	ctions		Geometric	
No.	Study	BRB modelling	Fatigue	gusset connection	Beam and column modelling	Column base	Beam	Gravity system	non-linear formulation	Damping model
П	Vafaei et al. [11]	Displacement-based fibre element with Giuffré-Menegotto-Pinto steel model	×	Moment- resisting	Force-based fibre element with Giuffré-Menegotto-Pinto steel model	Moment- resisting	Pinned	Pinned	$P-\Delta$ (small deformations)	5% Rayleigh
7	Chen [12]	Force-based fibre element with Giuffré-Menegotto-Pinto steel model	`	Moment- resisting	Force-based fibre element with Giuffré-Menegotto-Pinto steel model	Moment-resisting	Moment- resisting	Pinned	$P-\Delta$ (large deformations)	4% Rayleigh with tangent stiffness
8	Yu et al. [14]	Truss element with Giuffré-Menegotto-Pinto steel model	×	Moment- resisting	Force-based fibre element with Giuffré-Menegotto-Pinto steel model	Moment- resisting	Moment- resisting	Pinned	Linear	2% Rayleigh
4	Hu et al. [17]	Force-based fibre element with a user-defined material	×	Pinned	Force-based fibre element with Giuffré-Menegotto-Pinto steel model	Moment- resisting	Moment- resisting	Pinned	$P-\Delta$ (small deformations)	NA*
ιν	Prinz et al. [13]	Truss element with Giuffré-Menegotto-Pinto steel model	×	Pinned	Force-based fibre element with Giuffré-Menegotto-Pinto steel model	NA*	Pinned	Pinned	$P-\Delta$ (large deformations)	2% Rayleigh
9	Shayanfar et al. [18]	Force-based fibre element with Giuffré-Menegotto-Pinto steel model	`	Moment- resisting	Force-based fibre element with Giuffré-Menegotto-Pinto steel model	Moment- resisting	Moment- resisting	NA*	$P-\Delta$ (large deformations)	NA*
7	Charney et al. [19]	Truss element with Giuffré-Menegotto-Pinto steel model	`	Pinned	Force-based fibre element with Giuffré-Menegotto-Pinto steel model	Moment- resisting	Moment- resisting	Pinned	NA*	2.5% Rayleigh

TABLE 1 | (Continued)

						Beam-column	olumn			
				BRB to	,	connections	tions	•	Geometric	
No.	Study	BRB modelling	Fatigue	gusset connection	Beam and column modelling	Column base	Beam column	Gravity system	non-linear formulation	Damping model
∞	Pham et al. [20]	Displacement-based fibre element with Giuffré-Menegotto-Pinto steel model	×	Pinned	Force-based fibre element with Giuffré-Menegotto-Pinto steel model	Moment- resisting	Pinned	Pinned	$P-\Delta$ (large deformations)	5% Rayleigh
6	Gray et al. [21]	Truss element with Giuffré-Menegotto-Pinto steel model	×	Pinned	Beam with hinges with Giuffré-Menegotto-Pinto steel model	NA*	Moment- resisting	Pinned	$P-\Delta$ (large deformations)	2.5% Rayleigh
10	Zsarnóczay et al. [7]	Truss element with Zsarnóczay and Vigh steel model	`	Pinned	Elastic beam column element with modified Ibarra-Medina- Krawinkler plastic hinge model	Moment-resisting	Pinned	Pinned	$P-\Delta$ (large deformations)	NA*
п	Raul et al. [22]	Truss element with Zsarnóczay and Vigh steel model	`	Pinned	Elastic beam column element with modified Ibarra-Medina- Krawinkler plastic hinge model	Moment-resisting	Fixed— panel zone	Pinned	$P-\Delta$ (large deformations)	2% Rayleigh
12	Kuzucu et al. [23]	Force-based fibre element with Giuffré-Menegotto-Pinto steel model	`	Moment- resisting	Force-based fibre element with Giuffré-Menegotto-Pinto steel model	Moment- resisting	Moment- resisting	Pinned	$P-\Delta$ (large deformations)	2% Rayleigh
13	Upadhyay et al. [6]	Truss element with Giuffré-Menegotto-Pinto steel model and Pinching model	`	Pinned	Force-based fibre element with Popovics Concrete and reinforcing steel materials	Moment- resisting	Moment- resisting	Pinned	$P-\Delta$ (large deformations)	NA*
41	Huang et al. [24]	Truss element with Giuffré-Menegotto-Pinto steel model	`	Moment- resisting	Force-based fibre element with bilinear model	Moment- resisting	Pinned	Pinned	$P-\Delta$ (large deformations)	2% Rayleigh
15	15 Ghowsi et al. [8]	Force-based fibre element with hysteretic material	×	Pinned	Force-based fibre element with bilinear model	Moment- resisting	Pinned	Pinned	$P-\Delta$ (large deformations)	NA*

Abbreviation: NA*, information not available.

10969845, 2025, 11, Downloaded from https://onlinelbitury.wiley.com/doi/10.1002/eqe.4383 by Ministry Of Health, Wiley Online Library for rules of use; OA articles are governed by the applicable Creative Commons License and Conditions (https://onlinelbitury.wiley.com/crems-and-conditions) on Wiley Online Library for rules of use; OA articles are governed by the applicable Creative Commons License and Conditions (https://onlinelbitury.wiley.com/crems-and-conditions) on Wiley Online Library for rules of use; OA articles are governed by the applicable Creative Commons License and Conditions (https://onlinelbitury.wiley.com/crems-and-conditions) on Wiley Online Library for rules of use; OA articles are governed by the applicable Creative Commons License and Conditions (https://onlinelbitury.wiley.com/crems-and-conditions) on Wiley Online Library for rules of use; OA articles are governed by the applicable Creative Commons License and Conditions (https://onlinelbitury.wiley.com/crems-and-conditions) on Wiley Online Library for rules of use; OA articles are governed by the applicable Creative Commons License and Conditions (https://onlinelbitury.wiley.com/crems-and-conditions) on Wiley Online Library for rules of use; OA articles are governed by the applicable Creative Commons License and Conditions (https://onlinelbitury.wiley.com/crems-and-conditions) on Wiley Online Library for rules of use; OA articles are governed by the applicable Creative Commons (https://onlinelbitury.wiley.com/creative Commons (https://onlinelbitury.wi

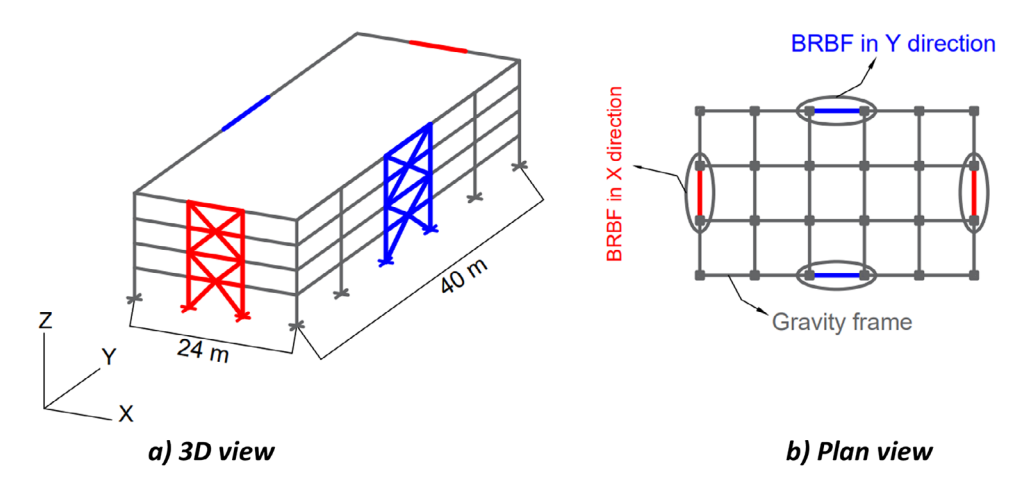


FIGURE 1 | Schematic of the case study four-storey steel BRBF building.

2.3 | Structural Damping

Structural damping is typically represented using the Rayleigh model with a 2% damping ratio assigned to the first and third modes. This damping model commonly uses either the initial or tangent structural stiffness matrix. Several studies have raised concerns with the use of the initial stiffness matrix in the Rayleigh damping model (e.g., Hall [30], Charney [31], Petrini et al. [32]), as it leads to spurious damping forces being produced during nonlinear deformations. As a result, using the tangent stiffness matrix might provide a more reasonable estimate of the damping forces (Petrini et al. [32]).

3 | Design of a Case Study Four-Storey Steel BRBF Building

Five practising engineers across Christchurch were interviewed to understand the current BRBF design practice adopted in New Zealand since no explicit guidance for their design is provided in NZS 3404 [33]. These efforts ensure that the adopted BRBF building design procedure is in line with the current industry practice. A Python-based automated script was developed to facilitate quick designs of plan-symmetric BRBFs based on NZS 1170.5 [34], NZS 3404 and the inputs from the practising engineers. This automated script was employed to design a four-storey steel BRBF building with a super-X configuration to investigate the impact of the out-of-plane buckling failure mode on its global seismic performance. The case study building was initially designed with steel moment resisting frames by Yeow et al. [35] for a site in Christchurch, New Zealand. In this study, the building has been re-designed with BRBFs as the lateral load resisting system (Figure 1).

The building has a rectangular floor plan measuring 24 m \times 40 m, as shown in Figure 1a. Four identical BRBFs are located along the building perimeter, as illustrated in Figure 1b. The first storey is 4.5-m tall, and all subsequent storeys are 3.6-m tall. The bays along both the X- and Y-directions are 8-m wide. The column base connections were designed to be moment-resisting, while shear tab connections were used for the beam-to-column connections. The bolted brace-to-gusset connections were designed using grade 8.8 bolts. Based on current design practice in New

Zealand, the equivalent static method of analysis was employed, incorporating the accidental eccentricity requirements specified in NZS 1170.5. The design ductility was assumed to be 4, and a structural performance factor (S_p) of 0.7 was used. The effective R-factor used in design is calculated as the ratio of k_μ to S_p , which equals 5.7 in this case. Here, k_μ corresponds to the design ductility factor adopted for this building. The engineers in New Zealand have begun to limit the μ used in design after the 2010/2011 Christchurch earthquakes, and hence, a μ value of 4 was recommended by the practising engineers in Christchurch.

The design details and BRBF member sizes are summarised in Table 2. The design process and calculations are described in detail in Sistla et al. [36]. The geometric and material properties of the steel sections used for the BRBF beams and columns are summarised in Onesteel hot rolled and structural steel tables [37]. The yield strength of both the BRB core and the gusset plates is 360 MPa. A yield strength overstrength factor of 1.1 is applied to the BRB core, while the tensile and compressive overstrength factors are 1.1 and 1.4, respectively. These factors are used to estimate the peak brace force at the ultimate limit state, which informs the capacity design of the gusset plates and BRBF frame members. The gusset plates were designed using Thornton's method, which idealises gusset plates as equivalent rectangular sections, in conjunction with an effective length factor of 0.7 and the NZS 3404 column curve.

4 | Numerical Models of the Case Study Building

Three BRBF building models were developed in OpenSeesPy, with their key features summarised in Table 3.

The 2D model represents the conventional BRBF modelling approach, which cannot simulate out-of-plane buckling failure of BRB gusset plates. It includes a pin-connected leaning gravity column that does not capture the behaviour of continuous gravity columns and completely excludes out-of-plane BRBF columns. Similar to the 2D model, the 3D Planar model represents a single BRBF within the building. It, however, addresses most of the limitations of the 2D model by incorporating a novel macro-model for the brace-to-gusset connection, along with two continuous leaning columns with plastic hinges that represent

TABLE 2 | Summary of design details of the case study four-storey steel BRBF building.

Method of analysis	Equivalent static
Site soil class	D
Importance level	2
Hazard factor (Z)	0.3 (Christchurch)
Fundamental period (T_1)	0.96 s (elastic 2D OpenSeesPy model)
Ductility factor (μ)	4
Structural performance factor (S_p)	0.7
Horizontal design action coefficient (C_d)	0.11
Peak storey drift at the design intensity level (ultimate limit state or ULS)	1.5%

	BRBF member section details				
Member	Location	Section (steel tables [37])			
Column	Storeys 1 and 2	350 WC 230			
Column	Storeys 3 and 4	350 WC 197			
Beam	Levels 1 and 2	530 UB 92.4			
Beam	Levels 3 and 4	530 UB 92.4			
BRB core	Storeys 1 and 2	Rectangular section—105 mm \times 30 mm			
BRB core	Storeys 3 and 4	Rectangular section—87 mm \times 20 mm			
Gusset plate	Storeys 1 and 2	Rectangular section—435 mm \times 425 mm \times 18 mm			
Gusset plate	Storeys 3 and 4	Rectangular section—385 mm \times 375 mm \times 14 mm			

TABLE 3 | Details of the BRBF models adopted.

		Modelling features					
Model name	Gusset plate Buckling	Out-of-plane BRBF columns	Continuous gravity system	Bidirectional loading	Fundamental period (s)		
2D	No	No	No	No	0.956		
3D Planar	Yes	Yes	Yes	No	0.955		
3D Spatial	Yes	Yes	Yes	Yes	0.952		

the gravity columns and the out-of-plane BRBF columns, respectively. Neither of these two models, however, can simulate response under bidirectional loading. In contrast, the 3D Spatial model explicitly represents all four BRBFs in the building, incorporates the effect of the floor slabs, and enables the simulation of response under bidirectional loading. These models, summarised in Table 3, incorporate progressively more realistic features of BRBF structures, thereby increasing both the complexity and computational demand of the analysis. These models are described in further detail below, and their results are compared to highlight their trade-offs in accuracy and computational efficiency.

The Rayleigh damping model using the tangent stiffness matrix was used to represent structural damping in all three models, with 2% damping calibrated to the first and third modes, as discussed in Section 2.3. Although the choice of damping model can influence the analysis results, this study focuses primarily on the comparative behaviour of the three models, minimising the

influence of the selected damping model on the conclusions of the study.

4.1 | 2D Model

The 2D model is representative of the conventional modelling approach and is illustrated in Figure 2. The BRB core was modelled using three displacement-based fibre elements with three integration points each, and the brace-to-gusset connection was represented using rigid elastic beam-column elements. The effective flexural rigidity of a BRB was computed by combining the flexural rigidities of the steel core and the concrete casing. The BRB core and restrainer assembly were modelled using a single hollow circular cross-section, with the diameter and thickness iteratively adjusted to match the flexural stiffness of the combined assembly while maintaining the required axial stiffness of the core. The Zsarnóczay and Vigh steel material model, in conjunction with a fatigue material model, was used to

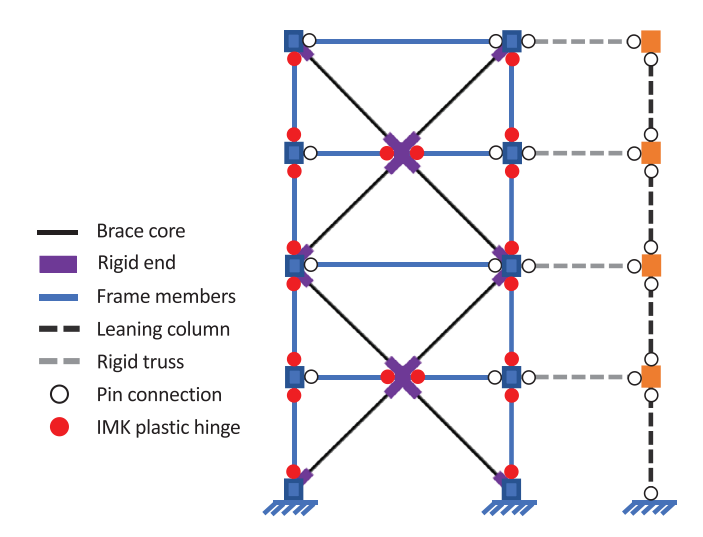


FIGURE 2 | Schematic of the 2D model.

represent the constitutive behaviour of the BRB core. Parameters of this material model were obtained from Table 3 of Zsarnóczay et al. [7]. The columns were modelled using elastic beam-column elements with concentrated plastic hinges at either end of the member. The modified IMK bilinear model was used to represent the hysteretic behaviour of the plastic hinges, and the model parameters were computed using the predictive equations proposed by Lignos et al. [28] for columns. The geometric properties of the steel sections required for this purpose were obtained from the Onesteel hot rolled and structural steel tables [37]. The beams were modelled with elastic beam-column elements with moment releases at the beam-column joints to represent shear tab connections. The hysteretic behaviour of the beam plastic hinges at mid-span was modelled using the modified IMK bilinear model, and the model parameters were computed using the predictive equation proposed by Lignos et al. [38] for beams. The BRBF column bases were fixed to represent the moment-resisting nature of the connections.

The gravity system was represented by a leaning column. All gravity columns within each storey were modelled using one elastic beam–column element with a cross-sectional area equal to the combined area of all the columns. The continuous effect of the gravity columns was ignored by pin-connecting the elements. The total gravity load in a storey was applied to the BRBF columns and the leaning column in proportion to their respective tributary areas. A large deformation $P\text{-}\Delta$ formulation was used to capture the second-order effects.

4.2 | 3D Spatial Model

The 3D Spatial model is illustrated in Figure 3. The model consists of four BRBFs along the perimeter, which are connected to four continuous corner leaning columns (labelled 1, 2, 3 and 4 in Figure 3) that represent the gravity system. Plastic hinges with a bilinear hysteretic behaviour and 1% strain hardening were placed at the ends of the leaning column at each storey. The leaning columns were connected to the BRBFs using rigid pinconnected truss elements, with pinned connections representing the shear tab gravity beam–column connections with negligible

moment resistance. The slabs were modelled using shell elements with an elastic membrane plate section and were connected to the four perimeter BRBFs and the leaning columns. The out-of-plane moments at their connections to the perimeter elements were released assuming composite slabs possess negligible post-cracking flexural stiffness.

An individual BRBF from the 3D Spatial model is illustrated in Figure 4a. Displacement-based fibre elements were used to model the BRB cores, end-zones and gusset plates, as illustrated in Figure 4b. The BRB core in this case was modelled using the same procedure as in the 2D model. The gusset plates were modelled with equivalent uniform cross-sections (illustrated in Figure 4b) and connected to the beam-column joints using rigid elements representing the flexurally rigid region of the gusset plates. The process to convert a gusset plate with a non-uniform cross-section into an element with a uniform cross-section is discussed in Section 4.2.1. Consistent with the 2D model, the Zsarnóczay and Vigh steel material model wrapped with a fatigue material was used to model the constitutive behaviour of the BRB core. The constitutive behaviour of the brace end-zones and gusset plates was modelled using the Giuffré-Menegotto-Pinto model. Studies by Zaboli et al. [39] and Sistla et al. [36] highlighted that initiating an asymmetric buckling mode requires less energy than initiating other modes. Therefore, out-of-plane geometric imperfections were introduced in opposite directions at both ends of each brace to simulate an asymmetric buckling mode (illustrated in Figure 4c), as this approach provides a conservative estimate of the gusset plate buckling load. An initial out-of-plane geometric imperfection of $L_{Gp}/1000$ was introduced at the interface of the gusset plates and the brace end-zones, where L_{Gp} denotes the length of the gusset plate. A clearance (s_c) of 1 mm was adopted at the interface of the brace end-zone and the BRB core. An imperfection of $2s_c + L_{Gp}/1000$ was applied at the interface, based on eq. 5 of Zaboli et al. [39].

4.2.1 | Calibration and Validation of the Equivalent Rectangular Gusset Plate Approximation

A gusset plate can typically be divided into two regions as follows: a flexible region and a rigid region, as illustrated in Figure 5c. Figure 5a, from a finite element simulation by Court-Patience et al. [40], illustrates the flexible region of the gusset plate (bounded by the two red lines) and the rigid region close to the beam–column joint (spanned by the yellow line). These regions can also be observed in Figure 5b, obtained from an experimental test conducted by Vazquez-Colunga et al. [41]. A simple method to estimate the effective width (b_w) and effective length (L_w) of the flexible region of the gusset plate is proposed in this study and illustrated in Figure 5d.

$$b_w = \left(\frac{b_1 + b_2}{2}\right) \tag{1}$$

$$L_w = \left(\frac{b_1 + b_2}{2}\right) \left(\frac{0.6L_{max}}{b_1}\right) \tag{2}$$

Considering the distance from the last bolt line (at the brace end-zone) to the beam-column joint (L_{max} in Figure 5d) for estimating L_w would be overly conservative, since the region

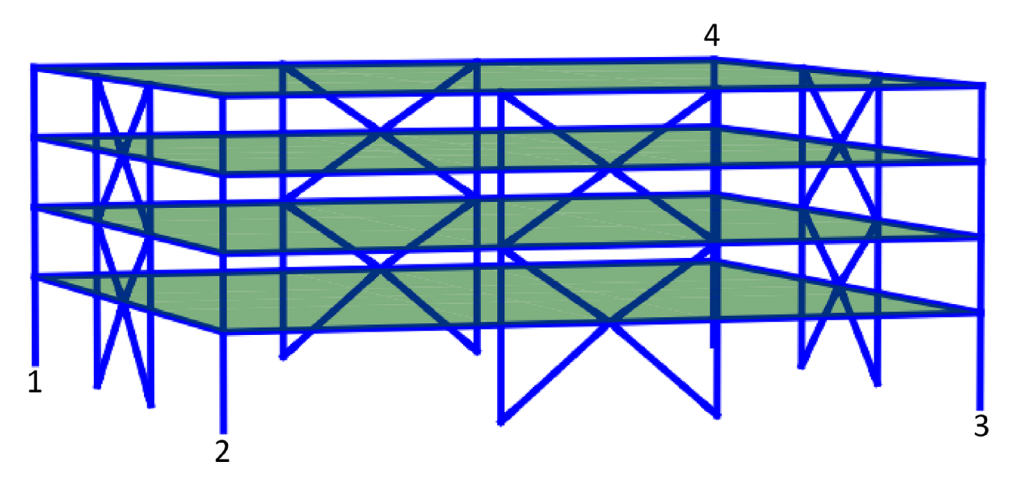


FIGURE 3 | Schematic of the 3D Spatial model.

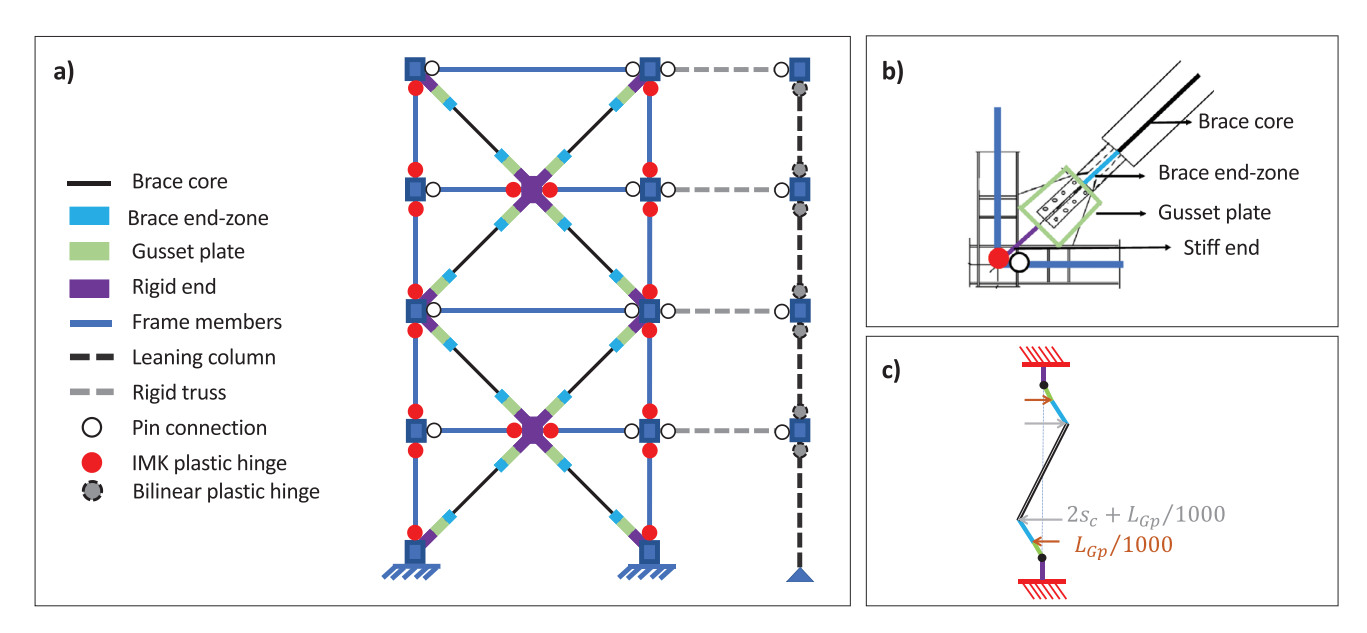


FIGURE 4 | Explicit modelling of the brace end-zone, gusset plate and rigid ends with geometric imperfections in the 3D Spatial model.

of the gusset plate close to the beam column joint is rigid (yellow line in Figure 5a). Values ranging from 0.2 L_{max} to 0.65 L_{max} were considered for the rigid end length, and 0.4 L_{max} was found to best represent the experimental results for a 3mm gusset plate, based on calibration to a one-storey BRBF test conducted by Vazquez-Colunga et al. [41]. The same rigid end length was then used to assess whether the modelling approach could capture the variation in gusset plate buckling load due to changes in gusset plate thickness (increased from 3 to 8 mm) and yield strength (Grade 350 for thicknesses less than 6 mm and Grade 300 for thicknesses equal to or greater than 6 mm). The buckling loads of three different gusset plates with thicknesses 4, 5 and 6 mm were experimentally determined by Vazquez-Colunga et al. [41], and these results were used to calibrate their 3D continuum finite element model. They then used this finite element model to numerically determine the buckling load of gusset plates with thicknesses ranging from 3 to 8 mm. The gusset plate buckling loads estimated by the macromodel proposed in this study are compared to the numerical and experimental estimates in Figure 6. The gusset plate buckling loads estimated by the proposed macro-model agree well with those from both the 3D continuum model and experimental results, with relative errors not exceeding 10%. Although the proposed macro-modelling approach was calibrated using a 3-mm gusset plate, it consistently performed well for thicknesses up to 8 mm. Therefore, this modelling approach is considered valid for gusset plate thicknesses between 14 and 18 mm, as used in the case study building (Table 2).

4.3 | 3D Planar Model

The 3D Planar model (illustrated in Figure 7) is an improved version of the 2D model that can capture the out-of-plane buckling of the gusset plates. The brace connections are explicitly modelled with out-of-plane imperfections, the gravity system is modelled using a continuous leaning column with bilinear plastic hinges, and the out-of-plane BRBF columns are modelled with an additional leaning column fixed at the base.

Each node in this model has 6 degrees of freedom, but the out-ofplane translation of the BRBF beam-column nodes is restricted.

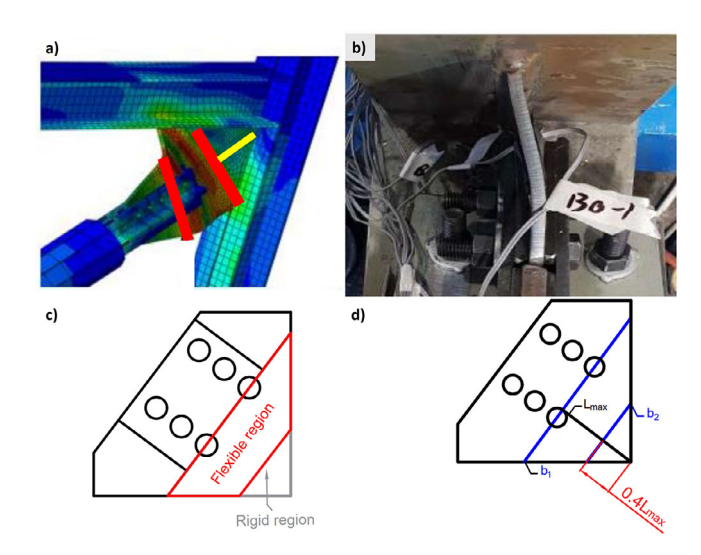
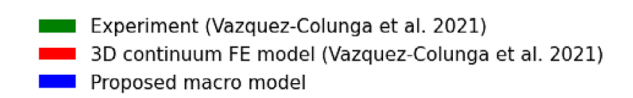


FIGURE 5 | (a) Effective buckling length from a finite element simulation by Court-Patience et al. [40]; (b) experimental tests by Vazquez-Colunga et al. [41]; (c) partitioning of a gusset plate into rigid and flexible regions; and (d) estimating the effective width and effective length of the flexible gusset plate region.



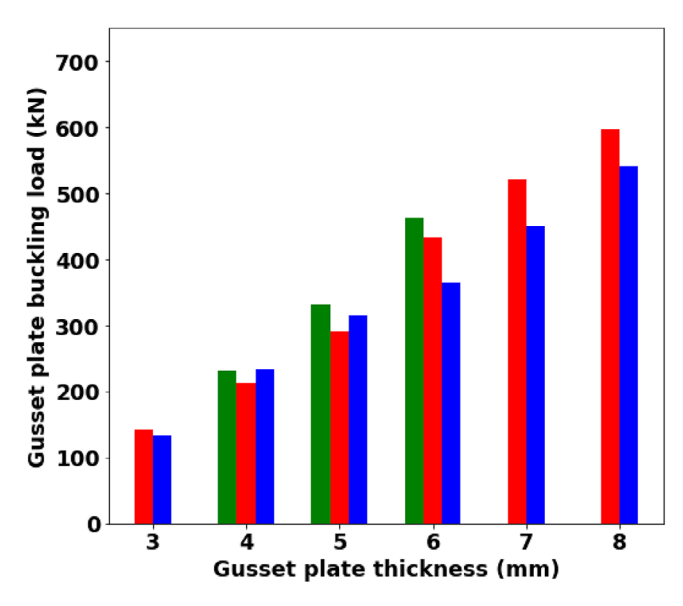


FIGURE 6 Comparison of gusset plate axial load capacities obtained from the proposed macro-model with experiments and 3D continuum finite element simulations conducted by Vazquez-Colunga et al. [41].

Out-of-plane buckling of the gusset plates is expected to produce bending about the weak axis of the beam to which the gusset plates are connected, as illustrated in Figure 8. This bending is resisted by the slab connected to the beam in the 3D Spatial model. As shown in Figures 7 and 8, this effect is captured in the 3D Planar model by introducing a weak axis bending restraint at the central beam nodes. Neglecting this slab restraint against minor axis beam bending can lead to premature buckling of the

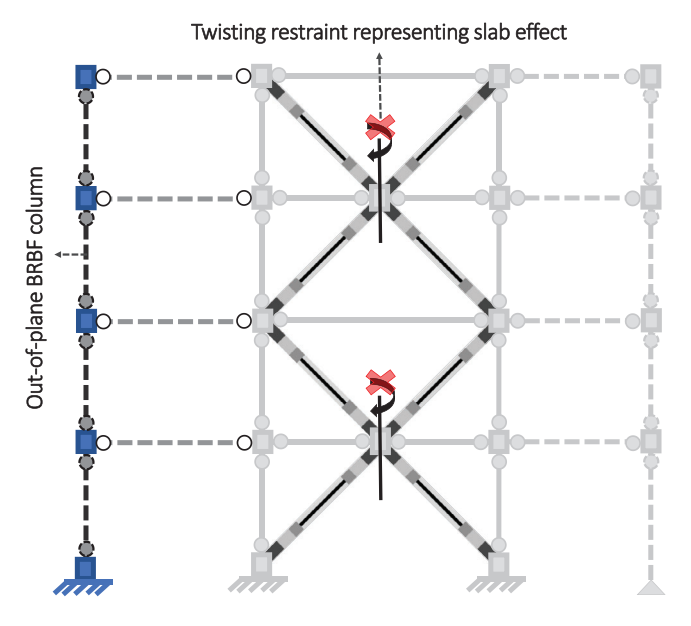


FIGURE 7 | Schematic of the improved BRBF model with computational efficiency (3D Planar model).

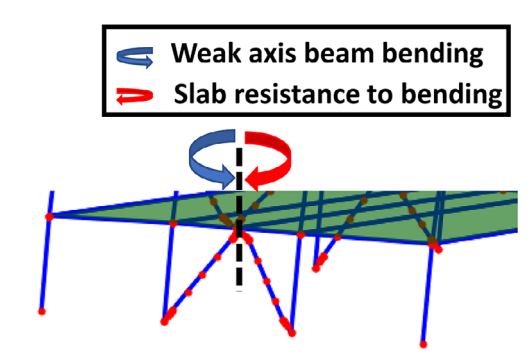


FIGURE 8 | Influence of the floor slab on the out-of-plane buckling of BRBs.

gusset plates, which is not likely to be representative of the actual behaviour.

5 | Non-Linear Static Analysis

The influence of gusset plate buckling on the performance of the case study BRBF building was investigated by first subjecting the three BRBF models to unidirectional and bidirectional non-linear static (pushover) analyses. Unidirectional pushover analysis was conducted on the three models by applying a load profile proportional to the fundamental mode shape in the direction of interest. Bidirectional pushover of the 3D Spatial model was conducted by first pushing it in the out-of-plane direction to a pre-defined building drift ratio, and then in the in-plane direction. Building drift ratio is defined as the ratio of the roof displacement to the total building height. Gusset plates are considered to have buckled when their out-of-plane displacement exceeds 5% of their length. Three demand parameters, namely, gusset plate strength ratio, building drift ratio at buckling, and in-plane storey drift ratio (SDR) at buckling, are used to quantify the influence of gusset plate buckling on the pushover response of the case study

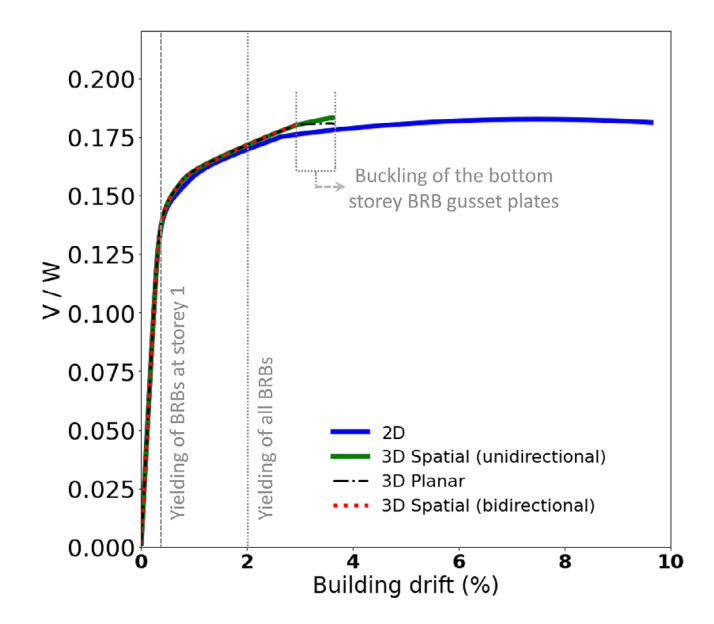


FIGURE 9 Pushover curves obtained from the three BRBF models subjected to unidirectional pushover analysis and the 3D Spatial model subjected bidirectional pushover with an out-of-plane building drift ratio of 3.0%.

building. The gusset plate strength ratio is defined as the ratio of peak compressive gusset plate force obtained from the numerical model (P) to the design capacity (P_{design}) predicted by the NZS 3404 (1997) gusset plate design procedure.

The pushover curves of the three models subjected to unidirectional pushover and the 3D Spatial model subjected to bidirectional pushover with an out-of-plane building drift ratio of 3.0% are illustrated in Figure 9. Yielding in the bottom storey BRBs was observed in all the models at a building drift ratio of 0.5%, whereas all remaining BRBs were observed to yield by a building drift ratio of 2.0%. The second-order effects of gravity loads are not significant in the 2D model because (i) the case study building has only four storeys, resulting in a moderate total building weight; and (ii) strain hardening of 0.5% in tension and 2.5% in compression was used in the Zsarnóczay and Vigh steel constitutive model for BRBs, effectively offsetting the P- Δ effects. The pushover curves obtained in this study are consistent with those reported for a six-storey steel BRBF building in a previous study by Zsarnóczay et al. [7].

The 2D model was able to deform up to a 10% building drift ratio without any significant loss of strength, as it cannot explicitly capture out-of-plane buckling of gusset plates. The performance of the 3D Planar model was found to be similar to the 3D Spatial model under unidirectional loading. Both the 3D Spatial and 3D Planar models deformed up to a 3.6% building drift ratio, at which point the gusset plates connected to the bottom storey compression brace buckled, leading to the termination of the analysis.

In both the models, the in-plane SDR at buckling of the bottom storey was observed to be 3.3%, while the gusset plate strength ratio was 0.77. This strength ratio indicates that the gusset plate buckling capacity observed from the pushover analysis is 77% of the capacity predicted by the design equation. Compared to the

unidirectional pushover of the 3D Spatial model, no significant reduction in the strength ratio was observed due to bidirectional interaction up to an out-of-plane building drift ratio of 2.5%. The gusset plate strength ratio decreased to 0.72 (a 6% reduction) and the in-plane SDR at buckling reduced to 2.8% (a 15% reduction) when the model was subjected to an out-of-plane building drift ratio of 3%. For reference, an out-of-plane building drift ratio of 3% is 82% of the in-plane SDR at the point of buckling observed from the unidirectional pushover analysis.

Thus, the pushover results indicate a reduction in building drift capacity from 10% to 3.6% due to gusset plate buckling under unidirectional loading, while no significant influence of bidirectional loading is observed.

6 | Non-Linear Dynamic Analysis

Multiple stripe analysis (MSA) was conducted using the three building models to investigate the influence of gusset plate buckling on the dynamic response of the case study building at nine ground motion intensity levels. Across the three models, 900 non-linear dynamic analyses were conducted using a parallel computing module based on a leader-follower architecture. A previously developed leader-follower module (https://github. com/luca-s/mpi-master-slave) was modified to conduct nonlinear dynamic analysis in parallel. The modified algorithm, along with detailed instructions on how to employ it for a simple cantilever system, can be found on the author's GitHub page (https://github.com/Saiteja802/parallel-MSA-openseespy). Bidirectional non-linear dynamic analysis of the 3D Spatial model was conducted by subjecting it to bidirectional ground motion record pairs simultaneously. In contrast, unidirectional nonlinear dynamic analysis of the 2D and 3D Planar models was conducted by subjecting them to ground motion records in the X and Y-directions independently. In both types of analysis, the structure is assumed to have collapsed if the peak SDR exceeds 10% in either the X- or the Y-direction. A collapse threshold of 10% peak SDR is justified by the expectation that the BRBs are likely to fracture and the gravity connections to fail by this point [42].

The computational cost of the 3D Spatial model was, on average, 150% higher than that of the conventional 2D model, while the 3D Planar model required approximately 60% more resources than the 2D model. It should be noted that the number of analyses conducted using the 2D and the 3D Planar models was twice that conducted using the 3D Spatial model. Further details regarding the processor type, number of cores and other specifications can be found in Sistla et al. [43]. The increased computational cost of the proposed models is attributed to the following reasons: (i) the 3D models have twice the number of entries in the element stiffness matrix for each member compared to the 2D model; and (ii) owing to the use of Newmark- β integration scheme (implicit method) for conducting dynamic analysis, the 3D models required significantly more iterations to achieve equilibrium at each increment, particularly at ground motion intensity levels that induced gusset plate buckling, which demanded substantially more iterations in the 3D models than in the 2D models.

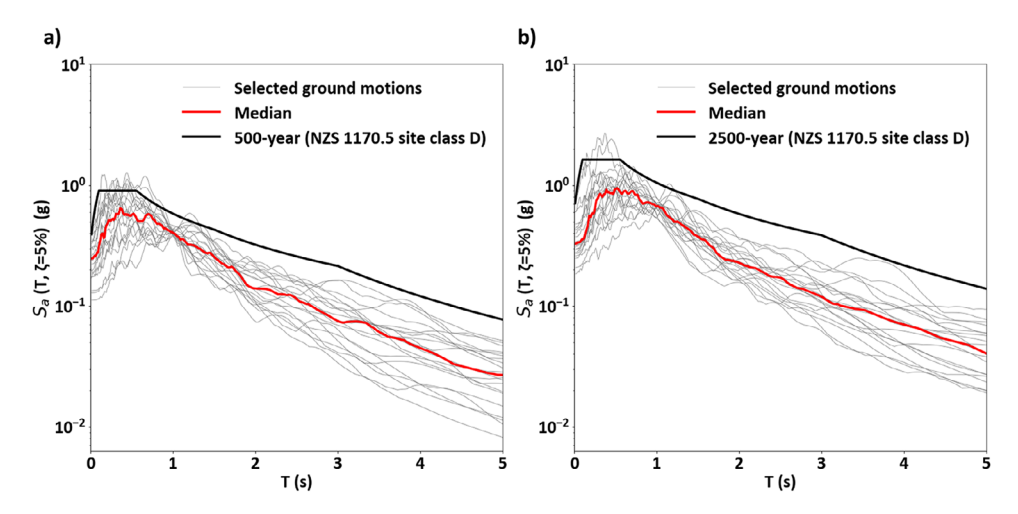


FIGURE 10 | Geometric mean of the acceleration response spectra in both directions at intensity levels corresponding to (a) 500-year return period, and (b) 2500-year return period.

The ground motion set adopted in this study was previously selected by Yeow et al. [35] for a site with soil class D in Christchurch. These ground motions were selected to match site-specific generalised conditional intensity measure (GCIM) targets [44]. Given that the fundamental period of the building is close to 1 s (Table 2), the ground motions selected by Yeow et al. [35], using the pseudo-spectral acceleration at 1 s as the conditioning intensity measure, are considered appropriate for this study. Further details related to the seismic source model, intensity measures, ground motion prediction equations and correlation relationships between various intensity measures can be found in Section 3.3 of Yeow et al. [35]. The geometric mean of the pseudo-acceleration response spectra in two orthogonal horizontal directions of the records selected at the 500-year and 2500-year return period intensity levels are illustrated in Figures 10a and b, along with the NZS 1170.5 uniform hazard design spectrum. The 500-year return period corresponds to the design intensity level of the case study building with an importance level of 2. The geometric mean spectra values at T =1 s (fundamental period of the structure) are generally lower than the NZS 1170.5 values, suggesting that the code estimates are conservative. As explained by Yeow et al. [35], this conservatism stems mostly from (i) overestimation of the effect of small-tomoderate earthquakes by the ground motion prediction equation on which NZS 1170.5 acceleration spectrum is based; and (ii) simplified spectral shape.

6.1 | Building Performance at the 500- and 2500-Year Return Period Intensity Levels

The building performance in terms of the peak SDRs, residual SDRs and peak floor accelerations (FAs), at the 500-year and 2500-year return period intensity levels is compared in Figures 11a and b, respectively. The maximum profiles of peak SDRs, residual SDRs and peak FAs along both the *X*- and *Y*-directions are illustrated in Figure 11. The peak SDRs, residual SDRs and peak FAs were found to be consistent across all three models up to the 2500-year return period intensity level. This is primarily attributed to the fact that gusset plate buckling was observed only beyond this intensity level in the 3D Spatial and 3D Planar

models. These results suggest that the observed engineering demand parameters show little to no sensitivity to the adopted modelling approach up to the 2500-year return period intensity level. Using a demolition threshold of 0.5% residual SDR, as recommended by Yeow et al. [35], the likelihood of building demolition is 15% at the design intensity level (500-year return period), increasing to around 50% at the 2500-year return period intensity level.

6.2 | Influence of Gusset Plate Buckling on Simulated Demands

In the 3D Spatial and 3D Planar models, buckling of gusset plates was observed only beyond the 2500-year return period intensity level. For all gusset plates that buckled in the BRBFs in either of the orthogonal directions, the gusset plate strength ratios (previously introduced in Section 5) from the 3D Spatial model and the 3D Planar model are plotted on the x-axis of Figure 12a, while the corresponding strength ratios from the 2D model are plotted on the y-axis. Collapse cases are shown in red, and non-collapse cases in blue. The plot indicates that 95% of the strength ratios in both the 3D Spatial and 3D Planar models are smaller than those from the 2D model. This suggests that gusset plate buckling reduces the gusset plate strength ratio and brace stiffness, leading to a decrease in storey strength and stiffness. A reduction in storey stiffness typically results in an increase in peak SDRs, as illustrated in Figure 12b. For all gusset plates that buckled in the BRBFs in either orthogonal direction, the peak SDRs from the 3D Spatial and 3D Planar models are plotted on the x-axis of Figure 12b, while the corresponding values from the 2D model are plotted on the y-axis. In 75% of the cases, the peak SDRs in the 3D models exceed those from the 2D model. No consistent trends, similar to those observed for the strength ratios and peak SDRs, were found for the peak FAs.

6.3 | Factors Influencing Gusset Plate Buckling

The strength ratios obtained from the 3D Spatial model and 3D Planar model were used to examine the impact of gusset

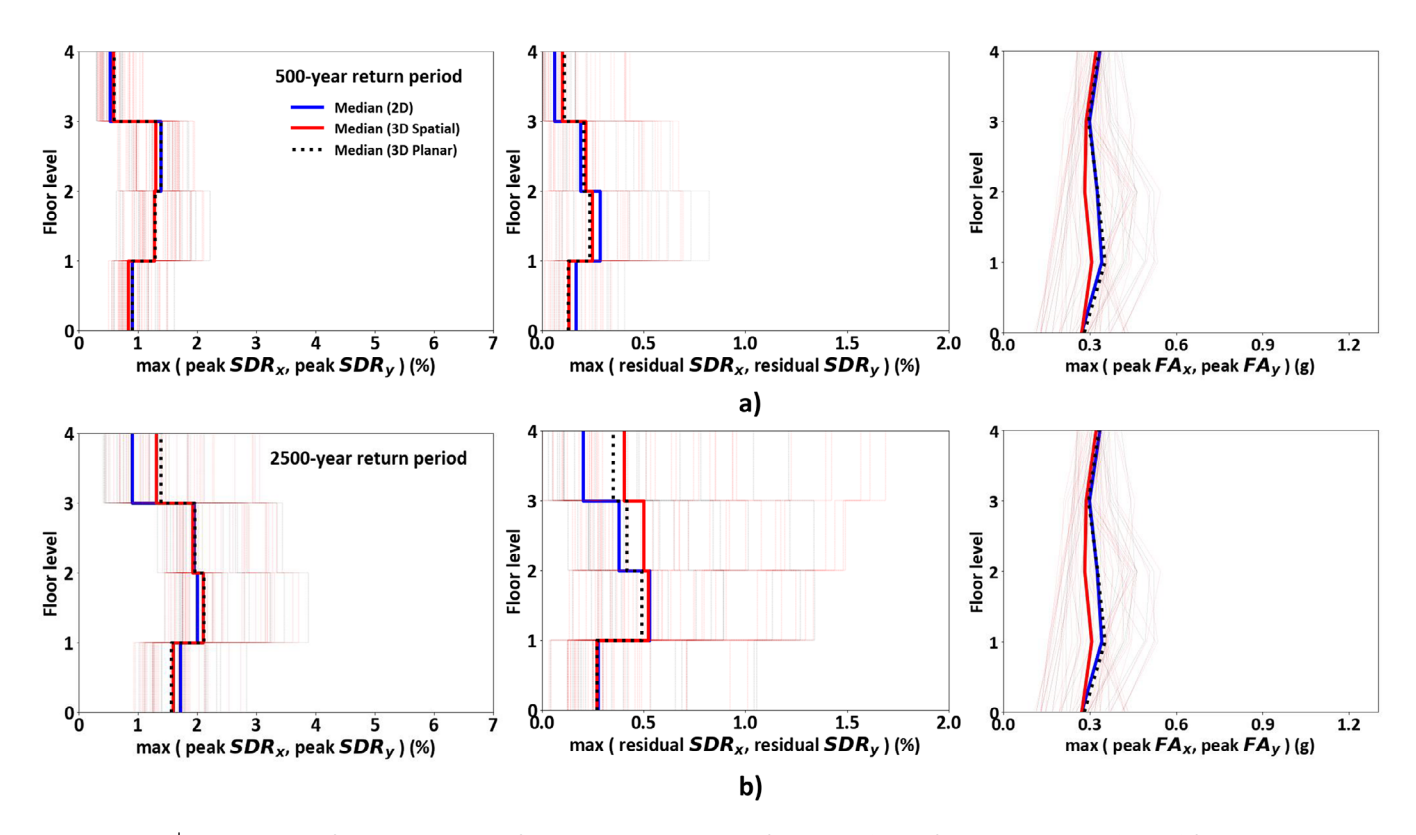


FIGURE 11 | Comparison of the peak storey drift ratios, residual storey drift ratios and peak floor accelerations obtained from the three BRBF models at intensity levels corresponding to (a) 500-year return period, and (b) 2500-year return period.

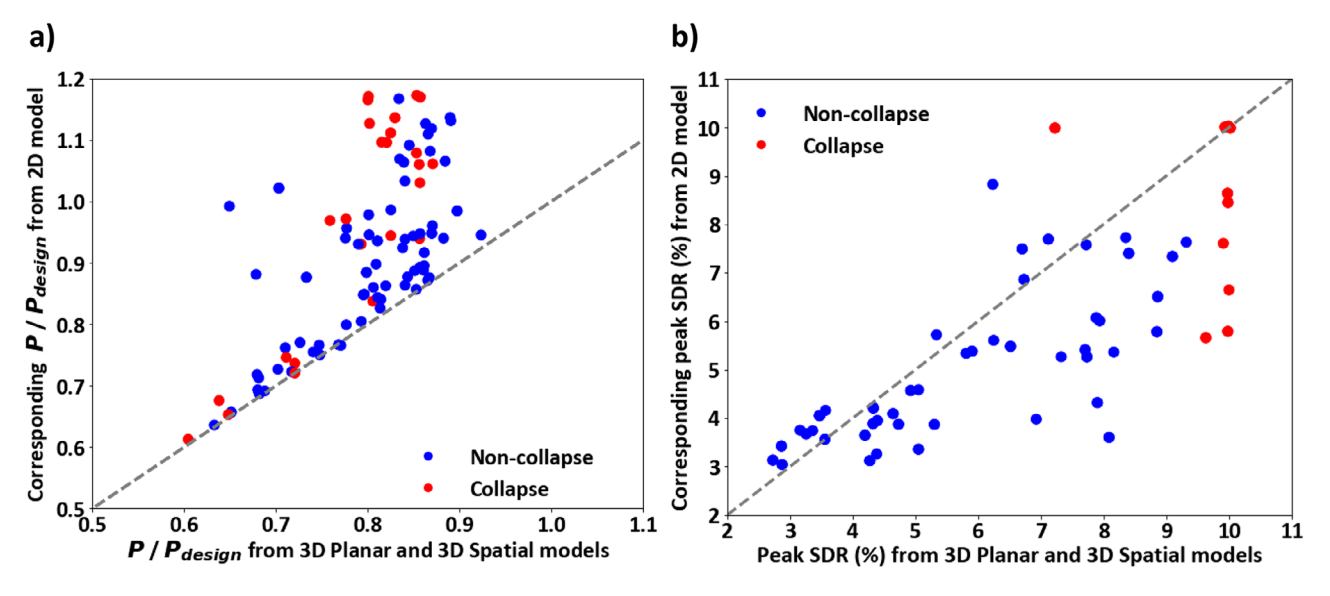


FIGURE 12 | Influence of gusset plate buckling on (a) gusset plate strength ratio (P/P_{design}) and (b) peak storey drift ratio.

plate position (mid-span vs. corner) and bidirectional interaction on out-of-plane buckling. Figure 13 illustrates two histogram plots of the gusset plate strength ratios obtained from non-linear dynamic analysis, categorised based on gusset plate position (Figure 13a) and model type (Figure 13b). A key observation from Figure 13 is that all observed strength ratios are less than one, indicating that the NZS 3404 (1997) method for designing gusset plates is unconservative. This aligns with previous observations by Vazquez-Colunga et al. [2] and Westeneng

et al. [5] and underscores the need for an improved design approach that effectively mitigates out-of-plane failure in BRB gusset plates. Several improved methods have been proposed in the literature to address these shortcomings (e.g., Zaboli et al. [39], Court Patience et al. [4]). Their efficacy in mitigating gusset plate buckling will be examined in a future study. The influence of ground motion uncertainty on gusset plate buckling capacity is highlighted by the variability observed in Figures 13a and b.

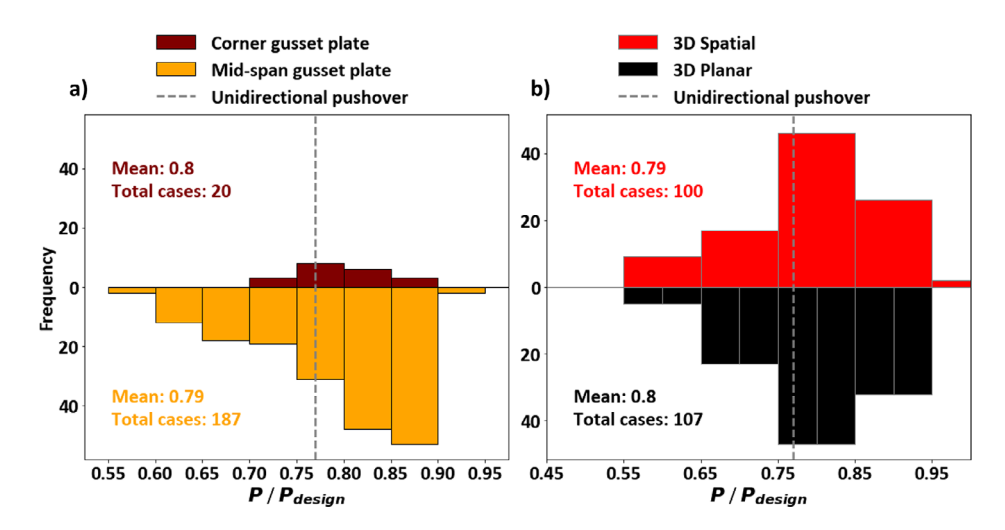


FIGURE 13 (a) Histogram of the gusset plate strength ratio (P/P_{design}) of corner and mid-span gusset plates; and (b) histogram of the gusset plate strength ratio (P/P_{design}) obtained from the 3D Spatial and 3D Planar models.

Figure 13a indicates that among all buckled gusset plates, approximately 10% are corner gusset plates, with the remaining 90% being mid-span gusset plates. While the mean strength ratio is similar in both cases, the lowest strength ratio among mid-span gusset plates is nearly 20% lower compared to that of corner gusset plates. The grey dashed line represents the gusset plate strength ratio obtained from a unidirectional pushover analysis. These findings are in line with the observations of Fussell [45], who concluded that mid-span gusset plates possess significantly less resistance to out-of-plane end rotation and are more likely to buckle when compared to corner gusset plates. As observed in Figure 13b, the total number of buckled gusset plates in the 3D Spatial model (100) and the 3D Planar model (107) were almost the same. Moreover, the average strength ratios were also similar, with values of 0.79 for the 3D Spatial model and 0.80 for the 3D Planar model. Since the 3D Spatial model considered bidirectional interaction while the 3D Planar model did not, these results further indicate that bidirectional loading has little to no influence on gusset plate buckling. This result is consistent with Court-Patience et al. [40], who based their observation on subassembly level experimental tests and 3D continuum finite element simulations.

Among all the instances of gusset plate buckling, 72% occurred with strength ratios greater than those predicted by unidirectional pushover analysis (grey dashed line in Figures 13a and b). Although buckling was observed in the bottom storey gusset plates during the unidirectional pushover, around 60% of buckling in the dynamic analysis occurred in the first storey, 40% in the second storey, with no buckling in the third and fourth storeys. These results indicate that although unidirectional pushover analysis provides a good starting point for understanding the influence of gusset plate buckling on the global seismic response of BRBFs, it does not provide a complete picture.

6.4 | Influence of Gusset Plate Buckling on Collapse Risk

Three lognormal collapse fragility curves were fit to the MSA results of each model and are illustrated in Figure 14a. These

TABLE 4 | Collapse fragility parameters and the mean annual frequency of collapse (λ_c) obtained from various BRBF modelling approaches.

Model	$\theta(\mathbf{g})$	$oldsymbol{eta}_{RTR}$	$oldsymbol{eta}_T$	λ_c
2D	2.24	0.50	0.67	0.76×10^{-4}
3D Planar	1.45	0.39	0.59	1.96×10^{-4}
3D Spatial	1.37	0.35	0.57	2.05×10^{-4}

fragility curves only account for the record-to-record uncertainty (β_{RTR}) . Modelling uncertainty (β_M) was incorporated into the lognormal standard deviation of the collapse fragility curves in Figure 14b (β_T) , as shown in Equation (3), leaving the median unchanged. A value of 0.45 was chosen to represent β_M based on the recommendations of Liel et al. [46]. The revised collapse fragility curves are illustrated in Figure 14b.

$$\beta_T = \sqrt{\left(\beta_{RTR}\right)^2 + \left(\beta_M\right)^2} \tag{3}$$

The parameters defining the collapse fragility curves obtained using all three models are summarised in Table 4. The 2D model produced the highest median collapse capacity (θ) estimate (2.24 g), followed by the 3D Planar model (1.45 g), and the 3D Spatial model (1.37 g). In comparison to the 2D model, the 3D Planar model exhibited a 35% reduction in θ , primarily due to gusset plate buckling. The 3D Spatial model demonstrated a further 5% reduction in θ compared to the 3D Planar model, attributed to bidirectional loading, but this difference is statistically insignificant.

The seismic hazard curve for the site computed by Yeow et al. [35] is illustrated in Figure 14b. The mean annual frequency of collapse (λ_c) for the case study building was estimated by integrating the product of the derivative of the hazard curve and each fragility curve. The λ_c values estimated using the three models are summarised in Table 4. The performance objectives outlined in NZS 1170.5 (2004) require the λ_c of the case study building to lie within the code-specified limits of 10^{-6} to 10^{-4} . The λ_c estimated by the 2D model is 0.76×10^{-4} , which falls within the

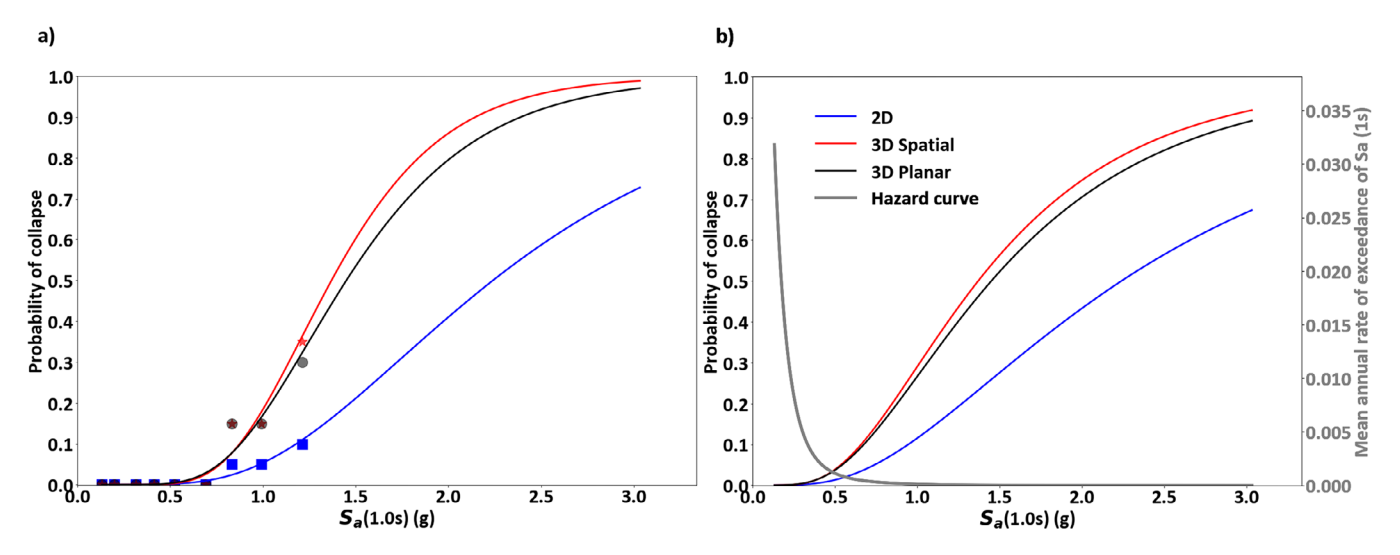


FIGURE 14 | (a) Collapse fragility curves derived from MSA results; and (b) modified collapse fragility curves including modelling uncertainty.

code-specified limits. The λ_c estimated by the 3D Planar model, however, is 1.96×10^{-4} , which exceeds the allowable range and is almost 150% greater than the estimate from the 2D model. This increase in collapse risk is mainly attributed to gusset plate buckling. The λ_c estimated by the 3D Spatial model is 4.5% greater than that of the 3D Planar model and 170% greater than that of the 2D model. Compared to the difference in λ_c estimated by the 2D and 3D Planar models, the difference between λ_c estimated by the 3D Planar and 3D Spatial models is negligible. Hence, the influence of bidirectional loading on λ_c is considered to be insignificant. These observations are based on the limited gusset plate slenderness ratios, thicknesses and brace configurations considered in this study. Further studies investigating these parameters are recommended to better understand the influence of bidirectional loading on gusset plate performance.

It should be noted that the 2D model consists of pin-connected gravity columns, which are representative of conventional modelling practice in research, whereas they were modelled as continuous columns in the 3D models to reflect their actual behaviour. Continuous gravity columns are known to redistribute drifts, potentially leading to a marginal increase in the structure's collapse capacity. Including this effect in the 2D model would marginally increase its collapse capacity and reduce the observed difference in collapse risk estimates between the 2D and 3D Spatial models, which currently stands at 170%. Although the design spectrum is conservative compared to the expected hazard (shown in Figure 10), gusset plate buckling still occurred, leading to an increased collapse risk. In regions where the code spectra are less conservative than those in New Zealand and the gusset plate design is similarly unconservative, the impact of gusset plate buckling on collapse risk is expected to be even more pronounced, potentially exceeding the 170% increase estimated in this study.

The observations from this study, conducted using a four-storey steel BRBF building, indicate that gusset plate buckling influences the structural response primarily at high seismic intensity levels and, therefore, is expected to affect collapse risk evaluation and scenario-based losses at these high intensity levels. A non-simulated collapse criterion, applied in post-processing by classifying all simulations with SDRs exceeding a defined

threshold as collapse cases, may be employed with the 2D model. However, this threshold, which is the SDR at gusset plate buckling, is sensitive to multiple factors, including brace configuration (e.g., super-X, chevron or diagonal), beam torsional stiffness in super-X and chevron configurations and gusset plate properties such as the thickness, slenderness ratio and yield strength. Developing such a collapse criterion would require a broad set of case study buildings that capture variability in these parameters, along with statistical models to predict gusset plate buckling drift ratios, given these parameters. Once such robust criteria are established, reliance on the computationally intensive 3D models proposed in this study may no longer be necessary.

7 | Conclusion

This study proposed a novel macro-modelling approach to capture the out-of-plane buckling of gusset plates in BRBF buildings. A case study four-storey steel BRBF building was designed in accordance with New Zealand seismic design standards, supplemented by guidance from practising engineers and modelled using the proposed approach. This model was subjected to both static pushover and dynamic analyses. The results indicate that the BRB gusset plate design method prescribed in NZS 3404 is unconservative in nature, with the code-prescribed procedures consistently predicting larger capacities than those observed in the analyses.

The drift capacity of the building inferred from the static pushover analysis decreased from 10% to 3.6% due to gusset plate buckling. Minimal influence of gusset plate buckling was observed on the global dynamic response of the building up to the 2500-year return period intensity level. Beyond this intensity level, though, gusset plate buckling led to an average 15% decrease in gusset plate strength ratio and a 20% increase in peak SDR. Assuming a residual SDR threshold of 0.5% for demolition, the results indicate that the likelihood of building demolition is 15% at the 500-year return period intensity level, increasing to 50% at the 2500-year return period intensity level. Finally, gusset plate buckling increased the mean annual frequency of collapse from 0.76×10^{-4} to 1.97×10^{-4} , which is 97% above the code-specified maximum

limit of 10^{-4} . Bidirectional loading was found to have minimal impact, further increasing the collapse risk by only 4.5%, to 2.05×10^{-4} . Of the buckled gusset plates, 10% were corner plates and 90% were mid-span plates, indicating that mid-span plates are more prone to buckling. These results emphasise the need for a better gusset plate design approach that effectively mitigates out-of-plane buckling, particularly of mid-span gusset plates.

Of the three types of models developed in this study, the 3D Spatial model offers a cost-effective alternative to 3D continuum models for global seismic performance assessment of BRBF buildings. For even greater efficiency, the 3D Planar model, which employs a few additional simplifying assumptions, serves as a viable substitute for the 3D Spatial model for analysis under unidirectional loading, as it consumes 37% fewer resources than the 3D Spatial model. For assessing BRBF performance up to the design intensity level though, conventional 2D models are sufficient. Since no significant bidirectional interaction effects on gusset plate performance were observed, the 3D Planar model is recommended for evaluating structural performance beyond the design intensity level. If gusset plate buckling is mitigated through future improvements to the design procedure, all three models should yield similar results. In this case, the conventional 2D model would be recommended at any intensity level due to its simplicity and computational efficiency.

Acknowledgments

Open access publishing facilitated by University of Canterbury, as part of the Wiley - University of Canterbury agreement via the Council of Australian University Librarians.

Data Availability Statement

The data that support the findings of this study are available from the corresponding author upon reasonable request.

References

- 1. M. Bruneau and G. MacRae, "Building Structural Systems in Christchurch's Post-Earthquake Reconstruction," *Earthquake Spectra* 35, no. 4 (2019): 1953–1978.
- 2. S. Y. Vazquez-Colunga, C. L. Lee, and G. A. MacRae, "Bidirectional Loading Performance of Gusset Plates in Buckling Restrained Braced Frames," *Engineering Structures* 242 (2021): 112521.
- 3. K. C. Tsai and P. C. Hsiao, "Pseudo-Dynamic Test of a Full-Scale CFT/BRB Frame—Part II: Seismic Performance of Buckling-Restrained Braces and Connections," *Earthquake Engineering & Structural Dynamics* 37, no. 7 (2008): 1099–1115.
- 4. D. Court-Patience and M. Garnich, "Buckling Analysis of Gusset Plates With Bolted Connections Using Finite Element Modeling," *Journal of Constructional Steel Research* 176 (2021): 106420.
- 5. B. A Westeneng, "Buckling Behaviour of Gusset Plates in Buckling-Restrained Braced Frames," Master's thesis, University of Canterbury (2016).
- 6. A. Upadhyay, C. P. Pantelides, and L. Ibarra, "Residual Drift Mitigation for Bridges Retrofitted With Buckling Restrained Braces or Self Centering Energy Dissipation Devices," *Engineering Structures* 199 (2019): 109663.
- 7. Á. Zsarnóczay and L. G. Vigh, "Eurocode Conforming Design of BRBF–Part II: Design Procedure Evaluation," *Journal of Constructional Steel Research* 135 (2017): 253–264.

- 8. A. F. Ghowsi and D. R Sahoo, "Seismic Performance of Nine-Story Self-Centering Buckling-Restrained Braced Frames," in *Structural Integrity Assessment: Proceedings of ICONS 2018* (Springer, 2020), 801–813.
- 9. G. Wei, M. R. Eatherton, H. Foroughi, S. Torabian, and B. W Schafer. Seismic Behavior of Steel BRBF Buildings Including Consideration of Diaphragm Inelasticity (2020).
- 10. A. Neuenhofer and F. C. Filippou, "Evaluation of Nonlinear Frame Finite-Element Models," *Journal of Structural Engineering* 123, no. 7 (1997): 958–966.
- 11. D. Vafaei, M. E. Shemshadian, and S. M Zahrai, "Seismic Behavior of BRB Frames Under Near Fault Excitations," in 9th US National and 10th Canadian Conference on Earthquake Engineering (2010).
- 12. C. H Chen, "Performance-Based Seismic Demand Assessment of Concentrically Braced Steel Frame Buildings," (PhD thesis, University of California, Berkeley, 2010).
- 13. G. S. Prinz and P. W. Richards, "Seismic Performance of Buckling-Restrained Braced Frames With Eccentric Configurations," *Journal of Structural Engineering* 138, no. 3 (2012): 345–353.
- 14. Y. J. Yu, K. C. Tsai, C. H. Li, Y. T. Weng, and C. Y. Tsai, "Analytical Simulations for Shaking Table Tests of a Full Scale Buckling Restrained Braced Frame," *Procedia Engineering* 14 (2011): 2941–2948.
- 15. M Menegotto, "Method of Analysis for Cyclically Loaded RC Plane Frames Including Changes in Geometry and Non-Elastic Behavior of Elements Under Combined Normal Force and Bending," in *IABSE Symposium on Resistance and Ultimate Deformability of Structures Acted on by Well Defined Repeated Loads* (1973).
- 16. P. Uriz, Toward Earthquake-Resistant Design of Concentrically Braced Steel-frame Structures (Pacific Earthquake Engineering Research Center, 2008).
- 17. J. W. Hu, D. H. Choi, and D. K. Kim, "Inelastic Behavior of Smart Recentering Buckling-Restrained Braced Frames With Superelastic Shape Memory Alloy Bracing Systems," *Proceedings of the Institution of Mechanical Engineers, Part C: Journal of Mechanical Engineering Science* 227, no. 4 (2013): 806–818.
- 18. M. A. Shayanfar, R. Zare Bidoki, B. Farhadi, and S. M Shahabi, "Assessment of Various Modeling Parameters and Their Influence on Seismic Behavior of Braced Steel Frame Structures," in *15th World Conference on Earthquake Engineering* (2012).
- 19. O. Atlayan and F. A. Charney, "Hybrid Buckling-restrained Braced Frames," *Journal of Constructional Steel Research* 96 (2014): 95–105.
- 20. H. Pham, Performance-Based Assessments of Buckling-Restrained Braced Steel Frames Retrofitted by Self-Centering Shape Memory Alloy Braces. PhD thesis, Georgia Institute of Technology (2013).
- 21. M. G. Gray, J. C. De Oliveira, C. C. Binder, C. Christopoulos, and J. I Binder, "Effects of Post-Yield Stiffening and Strengthening on the Collapse Performance of Non-Buckling Braced Frames," in *Tenth US National Conference on Earthquake Engineering* (2014).
- 22. S. R. Zaruma Ochoa, "Seismic Stability of Buckling-restrained Braced Frames" (Diss., University of Illinois at Urbana-Champaign, 2017).
- 23. I. B Kuzucu, "The Nature of the Vertical Distribution of Seismic Responses in Multi-Story Structures" (PhD thesis, University of Arizona, 2022).
- 24. Y. Huang, Q. Wu, and T. Tang, "Seismic Performance and Design of the Fully Assembled Precast Concrete Frame With Buckling-Restrained Braces," *Buildings* 12, no. 11 (2022): 1818.
- 25. A. Alghossoon and A. H. Varma, "Fiber-Based Model for Simulating Strength and Stiffness Deterioration of High-Strength Steel Beams," *Thin-Walled Structures* 183 (2023): 110432.
- 26. Y. Suzuki and D. G. Lignos, "Fiber-Based Hysteretic Model for Simulating Strength and Stiffness Deterioration of Steel Hollow Structural Section Columns Under Cyclic Loading," *Earthquake Engineering & Structural Dynamics* 49, no. 15 (2020): 1702–1720.

- 27. L. F. Ibarra, R. A. Medina, and H. Krawinkler, "Hysteretic Models That Incorporate Strength and Stiffness Deterioration," *Earthquake Engineering & Structural Dynamics* 34, no. 12 (2005): 1489–1511.
- 28. D. G. Lignos, A. R. Hartloper, A. Elkady, G. G. Deierlein, and R. Hamburger, "Proposed Updates to the ASCE 41 Nonlinear Modeling Parameters for Wide-Flange Steel Columns in Support of Performance-Based Seismic Engineering," *Journal of Structural Engineering* 145, no. 9 (2019): 04019083.
- 29. G. A MacRae, "The Continuous Column Concept-Development and Use," in *Proceedings of the Ninth Pacific Conference on Earthquake Engineering Building an Earthquake-Resilient Society* (2011).
- 30. J. F. Hall, "Problems Encountered From the Use (or Misuse) of Rayleigh Damping," *Earthquake Engineering & Structural Dynamics* 35, no. 5 (2006): 525–545.
- 31. F. A. Charney, "Unintended Consequences of Modeling Damping in Structures," *Journal of Structural Engineering* 134, no. 4 (2008): 581–592.
- 32. L. Petrini, C. Maggi, M. N. Priestley, and G. M. Calvi, "Experimental Verification of Viscous Damping Modeling for Inelastic Time History Analyses," *Journal of Earthquake Engineering* 12, no. S1 (2008): 125–145.
- 33. Standards New Zealand, NZS 3404:1997: Steel Structures Standard (1997).
- 34. Standards New Zealand, NZS 1170.5 Structural Design Actions Part 5: Earthquake Actions-New Zealand (2004).
- 35. T. Z. Yeow, A. Orumiyehei, T. J. Sullivan, G. A. MacRae, G. C. Clifton, and K. J. Elwood, "Seismic Performance of Steel Friction Connections Considering Direct-Repair Costs," *Bulletin of Earthquake Engineering* 16 (2018): 5963–5993.
- 36. S. Sistla, R. Chandramohan, and T. J Sullivan, "Modelling the Out-of-Plane Buckling Behaviour of BRBFs," in *Proceedings of the NZSEE Annual Conference* (2022).
- 37. Edcon Steel, Seventh Edition: Hot Rolled and Structural Steel Products, BlueScope Steel, 2021. [Online]. Available: https://www.edconsteel.com.au/wp-content/uploads/2021/09/seventh-edition-hot-rolled-and-structural-steel-products.pdf.
- 38. D. G. Lignos and H. Krawinkler, "Deterioration Modeling of Steel Components in Support of Collapse Prediction of Steel Moment Frames Under Earthquake Loading," *Journal of Structural Engineering* 137, no. 11 (2011): 1291–1302.
- 39. B. Zaboli, G. Clifton, and K Cowie, "Out-of-Plane Stability of Gusset Plates Using a Simplified Notional Load Yield Line Method," in *Proceedings of the NZSEE Annual Conference* (2017).
- 40. D. Court-Patience, Numerical Study on the Structural Performance of Buckling-restrained Braces and End Connections (University of Canterbury, 2021).
- 41. S. Y. Vazquez Colunga, Analysis and Design of Gusset Plates in Buckling-Restrained Braced Frames (Diss., University of Canterbury, 2020).
- 42. S. Shu, K. Dai, T. Li, A. El Damatty, and T. Sun, "Impact of Ground Motion Duration on Seismic Performance of Buckling Restrained Braced Frames," *Soil Dynamics and Earthquake Engineering* 174 (2023): 108197.
- 43. S. Sistla, R. Chandramohan, and T. J Sullivan, "Collapse Risk Assessment of a BRBF Building Considering the Out-of-Plane Buckling of Gusset Plates and Brace End-Zones," in *Proceedings of the Pacific Conference on Earthquake Engineering* (2023).
- 44. B. A. Bradley, "A Generalised Conditional Intensity Measure Approach and Holistic Ground-Motion Selection," *Earthquake Engineering & Structural Dynamics* 39, no. 12 (2010): 1321–1342.
- 45. A. Fussell, Heavy Brace Gusset Plate Connections for Braced Steel Frames (Steel Construction New Zealand Inc., 2011).
- 46. A. B. Liel, C. B. Haselton, G. G. Deierlein, and J. W. Baker, "Incorporating Modeling Uncertainties in the Assessment of Seismic Collapse Risk of Buildings," *Structural Safety* 31, no. 2 (2009): 197–211.